FINAL REPORT

Project title: **Advanced multi-wavelength ultrafast fiber lasers for stain free histopathology**

Principal investigator: Róbert Szipőcs, Ph.D.

Duration: 48 months (2018-09-01 - 2022-08-31)

Summary of our main results:

We upgraded our CARS imaging system for real time DVRF-CARS imaging using 2 NDD detectors parallel, which was used for generation of quasi hematoxylin-eosin stained real-time images of skin tumors (basalioma). IF-CARS imaging system of similar performance was developed and tested on brain slices with our partners at University of Szeged. An FPGA based data collection, processing and display system was developed for our IF-CARS and DVRF-CARS systems. Our microscope system was upgraded for mosaic imaging of fixed or frozen skin sections.

Optical fibers of different types were tested for distortion free fiber delivery of ultrafast laser pulses between the laser source and scanning head of the microscope. To this end, spectral bandwidth of our lasers were reduced down to 1-2 nm, which resulted 0.6-1.2 ps long pulses at the wavelengths of our interest: 790-810 nm, 920-940 nm and 1010-1030 nm. Two-photon excitation efficiency of our lasers is not degraded at all since their longer pulses were compensated by the lower repetition rate of the laser resulting in similar peak powers of the laser pulses. The 1-2 nm spectral bandwidth of our newly developed lasers results in higher spectral selectivity in CARS imaging (e.g. in case of lipid/protein imaging), while in case of fiber delivery, this reduced spectral bandwidth results in considerably lower dispersive effects without degrading imaging quality.

Results already published:

1. **Stain-free histopathology of basal cell carcinoma by dual vibration resonance frequency CARS microscopy.** Basal cell carcinoma (BCC) is the most common malignancy in Caucasians. Nonlinear microscopy has been previously utilized for the imaging of BCC, but the captured images do not correlate with H&E staining. Using coherent anti-Stokes Raman scattering (CARS) technique, we

developed a novel algorithm to post-process images obtained from dual vibration resonance frequency (DVRF) CARS measurements to acquire high-quality pseudo H&E images of BCC samples. We adapted our CARS setup to utilize the distinct vibrational properties of CH_3 (mainly in proteins) and CH_2 bonds (primarily in lipids). In a narrowband setup, the central wavelength of the pump laser is set to 791 nm and 796 nm to obtain optimal excitation. Due to the partial overlap of the excitation spectra and the 5–10 nm FWHM spectral bandwidth of our lasers, we set the wavelengths to 790 nm (proteins) and 800 nm (lipids). Nonresonant background from water molecules also reduces the chemical selectivity which can be significantly improved if we subtract the DVRF images from each other. As a result, we acquired two images: one for "lipids" and one for" proteins" when we properly set a multiplication factor to minimize the non-specific background. By merging these images, we obtained high contrast H&E "stained" images of BBC's. For more, see: https://link.springer.com/article/10.1007/s12253-017-0356-6

2. **Interferometric Spectral Modulation of sub-100-fs Pump Pulses for High Chemical Contrast, Background Free, Real Time CARS Imaging.** A simple, fast interferometric spectral modulation technique is proposed for nonresonant background suppression during CARS imaging. We demonstrate that the proposed setup is also suitable for real time stain-free histopathology of the brain. For more, see: https://opg.optica.org/abstract.cfm?uri=BRAIN-2018-JTh3A.29

3. **Characterization of DHEA-induced PCOS-model by CARS Microscopy.** The efficiency of *Origanum majorana* and *Mentha piperita* essential oil co-treatment was studied on DHEA-induced PCOS-model by analysis of lipid content changes in cumulus oocytes complexes by CARS and Bodipy fluorescence microscopy. For more, see: https://opg.optica.org/abstract.cfm?uri=OMP-2019-OW4D.6

4. **Quantitative Analysis on Ex Vivo Nonlinear Microscopy Images of Basal Cell Carcinoma Samples in Comparison to Healthy Skin.** BCC is the most frequent malignant neoplasm in the Caucasian population. There are several therapeutic options for BCC, but surgical excision is considered gold standard treatment. As BCCs often have poorly defined borders, the clinical assessment of the tumor margins can be challenging. Therefore, there is an increasing demand for efficient *in vivo* imaging techniques for the evaluation of tumor borders prior to and during surgeries. In the near future, nonlinear microscopy techniques might meet this demand. We

measured the two-photon excitation fluorescence (TPEF) signal of nicotinamide adenine dinucleotide hydride (NADH) and elastin and second harmonic generation (SHG) signal of collagen on 10 *ex vivo* healthy control and BCC skin samples and compared the images by different quantitative image analysis methods. These included integrated optical density (IOD) measurements on TPEF and SHG images and application of fast Fourier transform (FFT), CT-FIRE and CurveAlign algorithms on SHG images to evaluate the collagen structure. In the future, these novel image analysis methods could be integrated in handheld nonlinear microscope systems, for sensitive and specific identification of BCC. For more, see: https://link.springer.com/article/10.1007/s12253-018-0445-1

5. **Microglia monitor and protect neuronal function through specialized somatic purinergic junctions.** Microglia are the main immune cells in the brain and have roles in brain homeostasis and neurological diseases. Mechanisms underlying microglia–neuron communication remain elusive. Our partners identified an interaction site between neuronal cell bodies and microglial processes in mouse and human brain. For this, we developed a multi-wavelength nonlinear microscope imaging system comprising two ultrashort pulse lasers operating at 760 nm and 910 nm for imaging NADH and eGFP labelled microglia, respectively. For more, see: https://www.science.org/doi/10.1126/science.aax6752

6. **A 20 MHz, sub ps, Tunable Ti:sapphire Laser System for Real Time, Stain Free, High Contrast Histology of the Skin.** A 20 MHz repetition rate, sub ps Ti:sapphire (Ti:S) laser system is proposed for real time, high chemical contrast dual vibration resonance frequency (DVRF) CARS imaging of the skin suitable for *in vivo* histology. For more, see: https://opg.optica.org/abstract.cfm?URI=Microscopy-2020-MTh3A.4

7. **Fiber coupled, 20 MHz Repetition Rate, sub ps Ti:sapphire Laser for in vivo Nonlinear Microscopy of the Skin.** A fiber coupled, sub ps Ti:sapphire laser suitable for *in vivo,* stain free, 3D imaging of skin alterations is introduced. It is pumped by a low cost, 2.1 W pump laser and delivers 0.6 1 ps high peak power pulses optimized for fiber delivery. For more, see: https://opg.optica.org/abstract.cfm?uri=boda-2021-DF2A.5&origin=search

8. **Numerical Analysis on ex vivo Second Harmonic Generation Images of Collagen Structure of Unstained Basal Cell Carcinoma Sections.** FFT analysis on mosaic SHG images of basal cell carcinoma skin sections of different subtypes is presented. This analysis combined with two

photon auto fluorescence imaging might be useful for assessment of tumor borders. For more, see: https://opg.optica.org/abstract.cfm?uri=ecbo-2021-EW4A.9&origin=search

9. **Low concentration Phloxine B staining for high chemical contrast, nonlinear microscope mosaic imaging of skin alterations in pseudoxanthoma elasticum.** Pseudoxanthoma elasticum (PXE) is an autosomal recessive metabolic disorder characterized by ectopic mineralization of soft connective tissue. Histopathology findings include fragmented, mineralized elastic fibers and calcium deposits in the mid-dermis. Nonlinear microscopy (NLM) can be used for visualization of these histopathological alterations of the mid-dermis in PXE-affected skin sections. Upon introducing a normalized 3D color vector representation of emission spectra of three of the main tissue components (collagen, elastin and calcification) we found that due to their broad, overlapping emission spectra, spectral separation of emission from elastin and calcification is practically impossible in fresh-frozen or unstained, deparaffinized PXE sections. However, we found that the application of a low concentration *Phloxine B* staining after the deparaffinization process creates an imaging contrast for these two tissue components, which enables spectral decomposition of their fluorescence images. The obtained concentration maps for calcium deposits can be well suited for the determination of illness severity by quantitative analysis. For more, see: https://opg.optica.org/boe/fulltext.cfm?uri=boe-13-1-252&id=465719

Results to be published:

10. A tunable sub- ps Ti:sapphire laser operating at around 800 nm, 920 nm and 1000 nm has been tested for distortion free fiber delivery of 0.6 to 1.2 ps pulses for nonlinear microscope imaging of the brain. We found that using solid core, LMA fibers with core diameters above 12 microns allows high S/N ration multiphoton imaging at all of these wavelengths even at a fiber length of 2 m up to average powers of 100 mW at repetition rates of 69 MHz (or higher). Experiments we carried out at Nanyang Technological University, NTU Singapore in July, 2022. Results are to be published later this year.
11. **Low Reflection Loss Dispersion Compensation Scheme for Broadly Tunable sub-ps Solid State Lasers**. Combination of high (R>99.9%) reflection from an ion-beam sputtered ultrabroadband chirped mirror and Fresnel reflection from a wedged fused silica substrate forming a Gires-Tournois interferometer provides a wavelength independent, adjustable dispersion

compensation for broadly tunable sub-ps lasers such as Ti:sapphire. Results are to be published later this year.

12. **Development of FPGA based real time image processing and display for in vivo, real time histopathological imaging.** Precision, low noise PMT amplifiers, A/D conventers and FPGA based image processing and display system based on an FPGA were developed for real time histopathological imaging of the skin and the brain. Testing is in progress on fixed skin sections. Results are to be published when proper imaging data and videos are available.

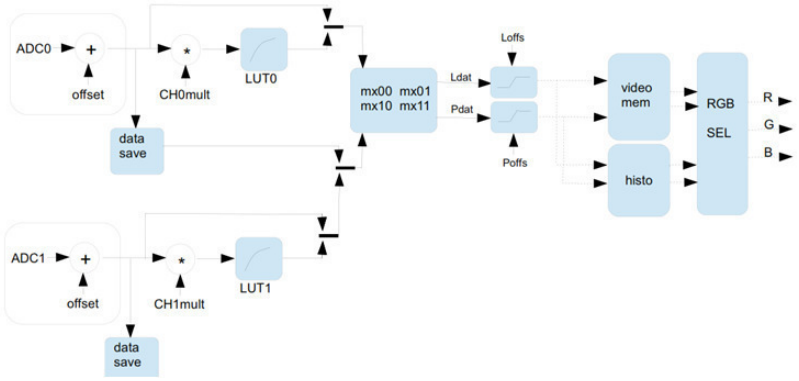

Operation of the FPGA modul. Input signals at ADC0 and ADC1 are generated by PMT-s installed for parallel lipid and protein detection by their anti-Stokes signal.

In the following pages, we enclose our conference papers that can not be reached directly from the links listed in our publication list.

Interferometric Spectral Modulation of sub-100-fs Pump Pulses for High Chemical Contrast, Background Free, Real Time CARS Imaging

Gábor Molnár[1], Ádám Krolopp[2], Norbert Kiss[3,4], Gábor Tamás[1], Róbert Szipőcs[2,4,*]
[1]*MTA-SZTE Research Group for Cortical Microcircuits, University of Szeged, Közép fasor 52, Szeged, H-6726, Hungary*
[2] *R&D Ultrafast Lasers Ltd, P.O. Box 622, H-1539 Budapest, Hungary*
[3]*Department of Dermatology, Venereology and Dermatooncology, Semmelweis University, Budapest, Hungary*
[4] *Wigner RCP, Institute for Solid State Physics and Optics, P.O. Box 49, H-1525 Budapest, Hungary*
* *r.szipocs@szipocs.com*

Abstract: A simple, fast interferometric spectral modulation technique is proposed for nonresonant background suppression during CARS imaging. We demonstrate that the proposed setup is also suitable for real time stain-free histopathology of the brain.
OCIS codes: (140.7090) Ultrafast lasers; (180.4315) Nonlinear microscopy.

1. Introduction

Coherent anti-stokes Raman scattering (CARS) [1] microscopy is widely used in label-free biomedical imaging applications. For *in vivo* diagnostic applications of CARS microscopy, wide field detection is preferred to descanned configurations [2]. Chemical selectivity poses a major difficulty when femtosecond pulse lasers are applied, since their spectral bandwidth is typically significantly higher (~5-10 nm) than the optimum value (~ 1 nm) matching the bandwidth of molecular vibrations. This fact leads to the appearance of an enhanced non-specific background and the decrease of spectral sensitivity in CARS imaging. In a recent publication, Li et al. [3] proposed a „multi-wavelength time-lens source" for nonresonant background suppression in a CARS imaging system utilizing a mode-locked Ti-sapphire laser (~100 fs, ~80 MHz) for the generation of the pump pulses. In their experiment, they used two picosecond pulse, Yb-fiber amplifiers that were synchronized with the Ti-sapphire laser. One of the Yb-amplifier was tuned "on resonance", the another "off resonance" relative to the CH_2 stretching frequency of 2845 cm^{-1}. Using the electronic pixel clock signal of their microscope, they were continuously switching between the resonant and anti-resonant Stokes lasers, so the recorded CARS image contained both the resonant and the anti-resonant CARS signals detected practically at the same time in subsequent pixels. In this way, after some post-processing of the image, the nonresonant background was successfully removed.

In this paper, we propose an alternative, fast (and cost efficient) spectral modulation technique for sub-100 fs pulse Ti-sapphire lasers, which allows us to modulate the laser spectrum on a ms time scale with the use of a piezo-driven Michelson interferometer. Switching between the properly shaped "on-resonance" and "off-resonance", laser spectra can be synchronized either to the electronic "line" or to the "frame" signals of our laser scanning microscope, which allows us to perform real time nonresonant background suppression during CARS imaging. In an alternative setting, we can modulate the relatively broad laser spectrum in such a way, that CARS imaging for "lipids" and "proteins" does not require any tuning of the pump (Ti-sapphire) laser or readjustment of the delay between the pump and Stokes (Yb-amplifier) pulses, which paves the way for real time stain-free histopathology [4].

2. Experimental setup

We used a CARS imaging setup similar to that was reported in Ref. 4. For our present studies, we constructed a small size Michelson interferometer (see Fig.1). In the beam path of the Ti:sapphire laser (inside our sealed *FemtoCARS Unit*), we replaced one of the 45 degree folding mirrors by our small size interferometer. One of its mirrors (M2) was placed on a piezo-electric linear actuator with a maximum travelling distance of 2.8 μm. The optical path difference (2*ΔL) had an offset value of ~0.1 mm, which resulted in different modulated laser spectra at the interferometer output depending on the phase difference of the two arms. We tested our setup for nonresonant background suppression at CH_2 stretching frequency of 2845 cm^{-1}, for which the laser central wavelength was set to 796 nm. Depending on the phase difference at the central wavelength, we were capable to generate "on resonance" and "off resonance" laser pulses with a spectral maximum or minimum at central wavelength (phase difference 0 or π in the interferometer). In this case, we faced the problem of different average power of the pump laser after the interferometer, that is why nonresonant background suppression required some post-processing of the images. For our stain-free histopathology imaging experiments [4] on in vitro brain slices, we used different interferometer

settings: we switched the phase difference between π/2 and - π/2 at the laser central wavelength of 975 nm. As a result we obtained two different laser spectra with maxima at 793 and 796 nm, respectively. In this latter case the power measured at the output of the interferometer was practically the same for the two different settings. In the following, we show representative images recorded from *in vitro* brain slices using the latter settings.

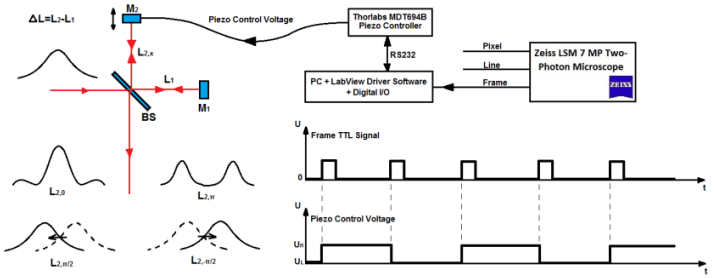

Fig. 1 A Michelson-interferometer is used for spectral modulation of the pump pulses. Depending on the electronically controlled phase difference of the two arms, different spectra can be generated for CARS imaging. ΔL has a properly set offset value depending on the spectral bandwidth of the laser applied. The phase difference is electronically controlled and synchronized to the frame (or line) signal of our microscope.

3. Results

Myelin sheaths - wrapping around the axons of neurons - are rich in lipid therefore we can record high quality 3D CARS images [5]. Degradation of the myelin sheath is the cause of neurodegenerative diseases, such as multiple sclerosis (MS), but a clear mechanistic understanding of myelin loss is missing. Previously we studied myelin breakdown in murine models with multiple sclerosis (MS) using the toxin cuprizone [5]. We found that myelin debris form lipid droplets alongside myelinated axon fibers. For quantification of lipid debris we used a custom-made software for segmentation and three dimensional reconstruction. For automatic lipid reconstruction, however, strong and specific lipid signal is needed. Therefore, to exclude CH_3 signal originating primarily from proteins and nonresonant background we introduced spectral modulation with our interferometer. In coronal brain slices of Wistar rat (P21, somatosensory cortex) we aimed to map and characterize lipid distribution in areas of layer 6 and in the lipid rich white matter tracks (Fig.2). We performed CH_2 (lipid) and CH_3 (protein) signal separation by spectral modulation tuning its peak from 793 nm to 796 nm using an interferometer (Fig.2, A,B). After subtracting images (CH_2-CH_3) we observed strong CH_2 contrast but less CH_3 contrast from white matter lipid structures. Using inverse image subtraction (CH_3-CH_2) we observed rich CH_3 contrast of the background neuropil and neuron somata, and less lipid structures from CH_2 vibration (Fig.2, C,D). Composite image shows minimal overlap of the images, which indicates more specific chemical selectivity (Fig.2, E).

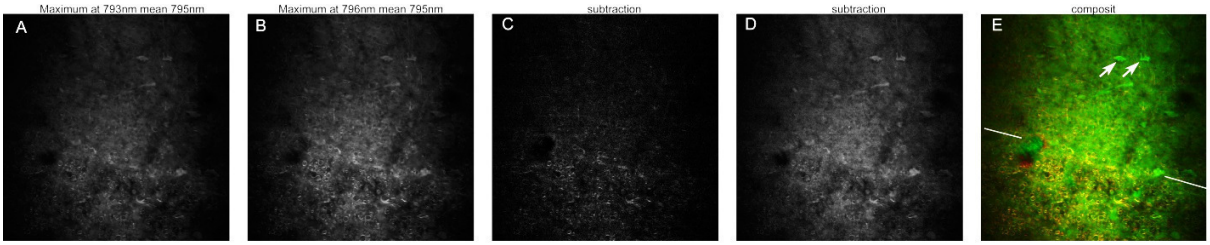

Fig. 2 IF-CARS imaging of *in vitro* brain slices of Wistar rat with a Mai Tai pump laser tuned to 795 nm. A-B) Images of somatosensory cortex coronal slices of layer 6 and white matter were recorded for two different, spectrally modulated pump pulses with spectral maxima at 793 nm ("CH_3") and 796 nm ("CH_2"). C) Subtraction of images (CH_2- CH_3) shown in Fig. 3 highlight more lipid structures. D) Inverse image subtraction (CH_3- CH_2) reveals protein rich background and somata of neurons. E) Composit image of lipid (red, CH_2- CH_3) and protein (green, CH_3-CH_2). Arrows show somata of neurons in layer 6, sidelong lines show the border of layer 6 and the white matter. Scalebar 50 μm.

4. References

[1] D. Haluszka, K. Lőrincz, N. Kiss, R. Szipőcs, E. Kuroli, N. Gyöngyösi, and N. Wikonkál, "Diet-induced obesity skin changes monitored by in vivo SHG and ex vivo CARS microscopy," Biomed. Opt. Express **7**, 4480–4489 (2016).
[2] A. Duarte, C. Schnedermann, P. Kukura, „Wide-Field Detected Fourier Transform CARS Microscopy," Scientific Reports **6**, 37516 (2016).
[3] B. Li, K. Charan, K. Wang, T. Rojo, D. Sinefeld, and Ch. Xu, "Nonresonant background suppression for coherent anti-Stokes Raman scattering microscopy using a multi-wavelength time-lens source," Opt. Express **24**, 26687-26695 (2016).
[4] N. Kiss, Á. Krolopp, K. Lőrincz, A. Bánvölgyi, R. Szipőcs, and N. Wikonkál „Stain-free Histopathology of Basal Cell Carcinoma by Dual Vibration Resonance Frequency CARS Microscopy," Pathol. Oncol. Res., published online, https://doi.org/10.1007/s12253-017-0356-6 (2017).
[5] A. Ozsvár, R. Szipőcs, Z. Ozsvár, J. Baka, P. Barzó, G. Tamás, and G. Molnár „Quantitative analysis of lipid debris accumulation caused by cuprizone induced myelin degradation in different cns areas," Brain Research Bulletin, accepted for publication (2017).

Characterization of DHEA-induced PCOS-model by CARS Microscopy

L. Fésűs[1,2], D. Domokos[4], V. Lener[4], T. Jakabovics[4], *R. Szipőcs[2,3,*], A. Kolonics[3,4]
[1]*Department of Dermatology, Semmelweis University, Budapest, Hungary*
[2]*Institute for Solid State Physics and Optics of Wigner RCP, P.O. Box 49, H-1525 Budapest, Hungary*
[3]*R&D Ultrafast Lasers Ltd, P.O. Box 622, H-1539 Budapest, Hungary*
[4]*BioFirmware Ltd, Berlini st. 47-49, H-1045 Budapest, Hungary*
* r.szipocs@szipocs.com

Abstract: The efficiency of *Origanum majorana* and *Mentha piperita* essential oil co-treatment was studied on DHEA-induced PCOS-model by analysis of lipid content changes in cumulus oocytes complexes by CARS and Bodipy fluorescence microscopy.
OCIS codes: (170.3880) Medical and biological imaging, (180.4315) Nonlinear microscopy.

1. Introduction

Polycystic ovary syndrome (PCOS) is one of most frequent female endocrine disorder, affecting 5%–10% of women, causing infertility, dysfunctional follicular maturation and ovulation, multicystic ovaries, hyperandrogenism. PCOS play a role in the enhancement of the risk of cardiovascular diseases and the development of diabetes [1]. Postnatal treatment of rodents with DHEA (Dehydroepiandrosterone) induced human PCOS characteristics of acyclicity, anovulation, polycystic ovaries, and hyperandrogenism: DHEA induces ovarian cysts and causes abnormal hormon level (increased serum testosterone, androstenedione and 5-α-dihydrotestosterone) similar to the women with PCOS [2]. Development of cysts causes an alteration of ovarian function and an imbalance in the oxidant–antioxidant balance [3]. Increased ROS within ovarian cells is associated with the impaired ovarian function [4]. DHEA transformed into potent estrogens such as estradiol and produces estrogenic effects of female sex hormone. Estradiol is involved in the regulation of the female reproductive cycles and responsible for the development of female secondary sexual characteristics such as the breasts, widening of the hips, and a feminine pattern of fat distribution in women. Mouse cumulus oocyte complexes (COCs) exhibit lipotoxicity responses in association with obesity or following treatment with high levels of *lipids in vitro* [5]. Traditional medicine, marjoram herb (*Origanum majorana*) tea was found to improve insulin sensitivity and reduce the levels of adrenal androgens in the hormonal profile of PCOS women in a randomised, double-blind, placebo-controlled trial [6]. Spearmint (*Mentha spicata)* has treatment potential on PCOS through inhibition of testosterone and restoration of follicular development in ovarian tissue) [7]. In our study we investigated the effects of pure 100 % natural essential oil mix of *Origanum majorana* and *Mentha piperita* in DHEA-induced PCOS-model by nonlinear microscopy.

2. Methods

4 week-old (~18 g) female C57 bl/6 mice (KinetoLab, Budapest, Hungary) were kept at 22 ± 2 °C under a 12 h light/12 h darkness cycle. The animals were fed normal diet and water was available *ad libidum*. C57BL/6 female mice were treated with dehydroepiandrosteron (DHEA) daily (6 mg/100 g body weight in 0,1 ml oil subcutan) for 20 consecutive days. The DHEA treated animals were randomized into different treatment groups (n=6). DHEA-K group and DHEA + Essential oil mix group. The latter group, after a DHEA treatment, was subsequently treated *per os* for 10 consecutive days with water solution of *Origanum majorana (150 mg/kg$^{body\ mass}$*, CAS 84082-58-6, Silvestris Ltd., Hungary*)* and *Mentha piperita (20 mg/kg$^{body\ mass}$,* CAS 8006-90-4, Azelis Ltd., Hungary*)* essential oils. After 20 days DHEA and 10 days Essential oil mix treatment, the mice were injected intraperitoneally (i.p.) with PMSG (pregnant mare's serum) at 5 IU/12 g of body weight, followed 48 h later by i.p. injection of hCG (human chorionic gonadotropin) at 5 IU/12 g of body weight. The ovaries were dissected and COCs were isolated from the oviducts at 16 h after hCG injection, placed in HEPES-buffered α-MEM (5 % FBS) and counted under microscope. The COCs were stained by Bodipy (Sigma-Aldrich) for lipid content or by MitoSOX Red (ThermoFischer Scientific), which is a mitochondrial superoxide indicator. During the staining procedure manufacturer's instructions was followed. After washing steps the COCs were fixed by paraformaldehide. We used a 2PEF and CARS imaging setup similar to that was reported in Ref. 8. For CARS-lipid imaging, we applied the CH_2 stretching frequency of 2845 cm^{-1}, for which the laser central wavelength was set to 800 nm in order to minimize the unwanted excitation of proteins. Note that our Stokes laser operates at 1030 nm [8]. For detections of

the 2PEF signal of the two different fluorescent labelling, two bandpass filters with green (500-550 nm, Bodipy) and orange (565-610 nm, MitoSOX Red) transmission bands were used.

3. Results

As a first step, we checked the co-localization of *Bodipy* fluorescent labelling and the detected CARS-lipid signal (see Fig.1). We found that even the small lipid droplets in the cells are clearly seen in both pictures. Interestingly, the CARS image shows slightly higher spatial resolution than the 2PEF image. As a next step, we compared the DHEA-induced changes of lipid content and ROS-level in COCs of murine PCOS-model by label-free CARS and MitoSox Red-labelled 2PE fluorescence microscopy (see Fig. 2). We found that DHEA treatment of female mice results in elevated lipid concentration of COCs parallel with increased mitochondrial ROS-production. Essential oil-mix treatment of mice decreased lipid and mitochondrial ROS-level in COCs.

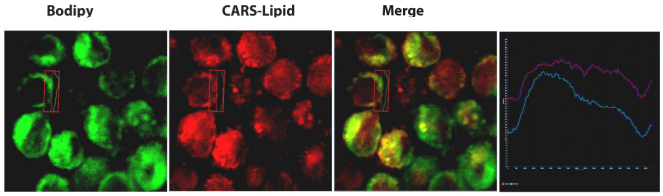

Fig.1. Bodipy staining is concentrated mainly into the cytosol, which shows a clear co-localization with the detected CARS-lipid signal. Interestingly, the CARS image shows slightly higher spatial resolution than the corresponding 2PEF image.

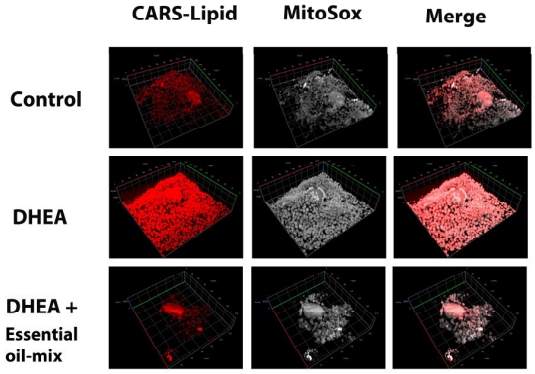

Fig. 2. Comparsion of DHEA-induced changes of lipid content and ROS-level in COCs of murine PCOS-model by label-free CARS and MitoSox Red-labelled 2PE fluorescence microscopy.

Concluding our results we can say that an increased dose of DHEA treatment resulted in PCOS escorted with elevated abdominal adipose tissue and liver weight (data not shown here) parallel with increased lipid-levels in COCs and elevated ROS-production. Essential oil-mix treatment resulted in decreased level of lipid and ROS in the cells. Label-free CARS imaging has been found to be a good alternative for Bodipy staining of lipids. Accordingly, CARS imaging might be a plausible approach to examine the effects of drugs on murine PCOS DHEA-model.

4. References

[1] D.H. Abott, et al. „Developmental origin of polycystic ovary syndrome-a hypothesis,.*"* J Endocrinology,. **174**, 1-5 (2002).
[2] V. Sander, et al. „Role of the N, N'-dimethylbiguanide metformin in the treatment of female prepuberal BALB/c mice hyperandrogenized with dehydroepiandrosterone," Reproduction **131**, 591-602 (2006).
[3] C.G. Luchetti, et al. „Effects of dehydroepiandrosterone on ovarian cystogenesis and immune function," J Reproductive Immunology. **64,** 59-74. (2004).
[4] A.B. Motta, et al. „*The involvement of nitric oxide in corpus luteum regression in the rat: feedback mechanism between prostaglandin F2α and nitric oxide,"* Molecular Human Reproduction,. **5**, 1011-1016 (1999).
[5] L.L. Wu, et al., „High-fat diet causes lipotoxicity responses in cumulusoocyte complexes and decreased fertilization rates," Endocrinology **151**, 5438-5445 (2010).
[6] L. Haj-Husein, et al. "The effect of marjoram (Origanum majorana) tea on the hormonal profile of women with polycystic ovary syndrome: a randomised controlled pilot study," J Human Nutrition Diet **29**, 105-111 (2016).
[7] A.M. Sadeghi, et al. „Role of Essential Oil of Mentha Spicata (Spearmint) in Addressing Reverse Hormonal and Folliculogenesis Disturbances in a Polycystic Ovarian Syndrome in a Rat Model," Adv. Pharm. Bull. **7**, 651-654 (2017).
[8] D. Haluszka, K. Lőrincz, N. Kiss, R. Szipőcs, E. Kuroli, N. Gyöngyösi, and N. Wikonkál, "Diet-induced obesity skin changes monitored by in vivo SHG and ex vivo CARS microscopy," Biomed. Opt. Express **7**, 4480–4489 (2016).

A 20 MHz, sub-ps, Tunable Ti:sapphire Laser System for Real Time, Stain Free, High Contrast Histology of the Skin

Luca Fésűs[1,2], Ádám Krolopp[1,3], Gábor Molnár[4], Norbert Kiss[1,2], Gábor Tamás[4], Róbert Szipőcs[1,3,*]

[1] *Wigner RCP, Institute for Solid State Physics and Optics, P.O. Box 49, H-1525 Budapest, Hungary*
[2] *Department of Dermatology, Venereology and Dermatooncology, Semmelweis University, Budapest, Hungary*
[3] *R&D Ultrafast Lasers Ltd, Konkoly-Thege str 29-33, H-1121 Budapest, Hungary*
[4] *MTA-SZTE Research Group for Cortical Microcircuits, University of Szeged, Közép fasor 52, Szeged, H-6726, Hungary*
* *r.szipocs@szipocs.com*

Abstract: A 20 MHz repetition rate, sub-ps Ti:sapphire (Ti:S) laser system is proposed for real time, high chemical contrast dual vibration resonance frequency (DVRF) CARS imaging of the skin suitable for *in vivo* histology.
OCIS codes: (140.7090) Ultrafast lasers; (180.4315) Nonlinear microscopy.

1. Introduction

Coherent anti-stokes Raman scattering (CARS) [1] microscopy is widely used in label-free biomedical imaging applications. For *in vivo* diagnostic use of CARS microscopy, wide field detection is preferred to descanned configurations [2]. Chemical selectivity poses a major difficulty when femtosecond (fs) pulse lasers are applied, as their spectral bandwidth is typically significantly higher (~5-10 nm) than the optimum value (~ 1 nm) matching the bandwidth of molecular vibrations. This fact leads to the appearance of an enhanced non-specific background and the decrease of spectral sensitivity in CARS imaging. Two years ago we proposed a fast spectral modulation technique for sub-100 fs pulse Ti:S lasers [3], which allowed us to modulate the laser spectrum on ms time scale with the use of a piezo-driven Michelson interferometer. In one of the settings we used, we modulated the laser spectrum of our laser in such a way, that CARS imaging for CH_2 bonds in "lipids" and CH_3 bonds "proteins" did not require any tuning of the pump (Ti:S) laser or any readjustment of the delay between the pump and Stokes (Yb-amplifier) pulses, which allowed us to record stain-free histological images [4] of brain slices. In this paper we report on a newly developed, ~20 MHz, sub-ps Ti:sapphire laser system, which supports real time, two-channel, high chemical contrast, DVRF CARS imaging, i.e. histology of the skin by a commercial LSM 7 MP microscope (Carl Zeiss, Jena, DE) without any modification of its ZEN software or postprocessing of the images like in case of our previous CARS setups used for histology [3,4].

2. Experimental setup

For our comparative studies, we used two different CARS imaging setups, as shown in Fig.1. In our setup at the University Szeged (USZ) [3,5], we used a ~80 MHz, ~80 fs Ti:S laser (*Mai Tai*, Newport Spectra-Physics, USA) as a pump laser (for details, see Refs. 3 and 5). In the setup at Wigner RCP, Budapest [1,4], we replaced our ~76 MHz, ~150 fs Ti:S laser by a newly developed, ~ 20 MHz repetition rate, sub-ps Ti:S laser (*FemtoRose 300 TUN LC*, R&D Ultrafast Lasers Ltd.). The long cavity laser configuration was similar to that was published in Ref. 6, with a few modifications, among them the most critical was the following: we replaced the SF10 prism pair by a Gires-Tournois interferometer, which provided considerably higher intracavity dispersion than the prism pair previously used. Beside a birefringent tuning element, fine tuning of the Ti:sapphire laser was obtained by the piezo controlled GTI. In our new setup, the spectral bandwidth of the pump (Ti:S) laser was reduced from 6-8 nm to ~2 nm. Accordingly, the pulse duration increased from ~150 fs to ~ 600 fs, or slightly above. This four-fold reduction in the peak intensity was compensated by the lower repetition rate of our long cavity Ti:sapphire laser comprising a Herriott-cell and a ~2W average power, 532 nm pump laser [6]. Pulse duration of the ~20 MHz laser was characterized by a PulseCheck autocorrelator (APE GmbH, DE). Depending on the intracavity dispersion set by the mirror spacing of an intracavity GTI, the pulse duration could be set in the 0.6-1 ps range. Spectral bandwidth of the ~20 MHz Ti:sapphire laser (pump) was measured $\Delta\lambda < 2$ nm allowing high spectral resolution DVRF-CARS imaging. For higher spectral contrast between the anti-Stokes signals generated by „lipids" and „proteins", we placed a Michelson interferometer similar to that was used in Ref. 3 into the beam path of our Stokes (Yb) laser. By spectral modulation, we obtained a double peaked spectrum with a peak separation of 5-6 nm at around 1030 nm. DVRF CARS imaging was performed by two NDD detectors of our microscope: the anti-Stokes signals for „lipids" and „proteins" were separated by a dichroic mirror with a long pass edge at around 645 nm, while two bandpass filters with central wavelengths at 641 nm and 650 nm were respectively placed in front of the NDD-s.

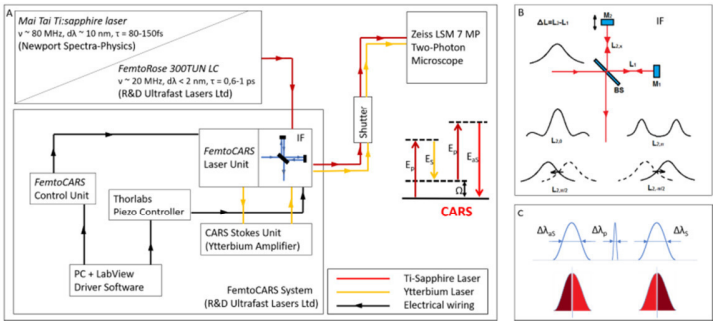

Fig. 1 A) Layout of the experimental setups used for IF-CARS [3] and real time DVRF CARS imaging with a 20 MHz, sub-ps Ti:S laser. In both setups, a Michelson-interferometer is used for spectral modulation of either the pump (IF-CARS setup, [3]) or Stokes pulses (real time DVRF CARS setup). By electonically modulating the phase difference ($\Delta\varphi$) of the two mirrors, different output spectra can be obtained. B) Phase difference $\Delta\varphi = 0$ at the central frequency results in a narrower spectrum, whereas $\Delta\varphi = \pi$ results in a double-peaked spectrum around the central wavelenght, when the path difference offset, ΔL is properly set. When the phase difference is $\pi/2$ or $-\pi/2$, two different spectrally shifted laser spectra is obtained with two maxima a few nm-s apart [3]. C) For high chemical contrast, real time DVRF-CARS imaging with two parallel NDD detectors, at least one of the pump or Stokes laser spectral bandwidth has to be small enough (< 2 nm) to create properly distinguishable anti-Stokes signals. If $\Delta\lambda_p$ is small (~2 nm) and $\Delta\lambda_S$ is broader (~10 nm), nearly half of the Stokes photons (of lower energy) excites the CH_2 bonds in lipids, while others (of higher energy) excite the CH_3 -bonds in proteins.

The optical signal detected by the „lipid" detector was pseudo-colored red, while that of the „protein" was given the color blue to match conventional H&E stained histology.

3. Results

Histological imaging experiments on *ex vivo* human and murine skin samples by different CARS imaging methods are summarized in Fig.2. As a main result, we can say that our new, ~20 MHz, sub-ps Ti:S laser system supports real time, two-channel, high contrast, dual vibration resonance frequency (DVRF) CARS imaging, i.e. histology of the skin by a LSM 7 MP microscope with its original ZEN software, with properly chosen commercial bandpass and dichroic filters in front of the two NDD detectors and without any postprocessing of the images like in case of our previous CARS setups used for histology [3,4]. This new setup can also be used for *in vivo* experiments on murine skin or *ex vivo* analysis on human pathological skin samples, which, in longer term, may pave the way for applications during Mohs-surgery or real time *in vivo* diagnosis of skin lesions.

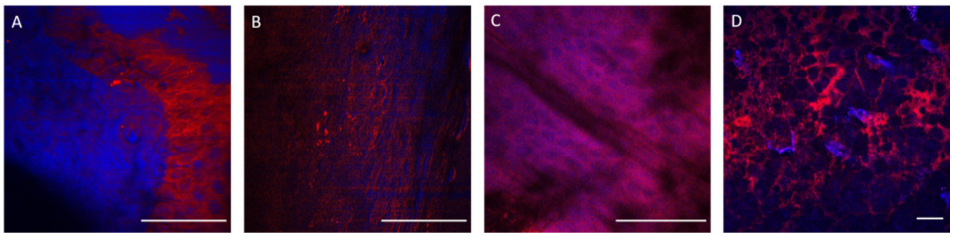

Fig. 2 Histological imaging of *ex vivo* human and murine skin samples by different CARS imaging methods. A) Composite of CARS images recorded for „proteins" and „lipids" in human basal cell cancer (after post-processing) with a Mai Tai pump laser tuned to 790 and 798 nm, respectively [4]. B) IF-CARS imaging of murine skin (after post-processing) with spectrally modulated Mai Tai pump laser pulses with spectral maxima az 792 and 796 nm [3]. C) Post-processed DVRF-CARS image of murine skin with a Mai Tai pump laser tuned to 796 nm with simultaneous detection of the two anti-Stokes signals. D) Real time DVRF-CARS image of murine skin with simultaneous detection of the lipid („-CH_2 vibration") and protein („-CH_3 vibration") channels with a FemtoRose 300TUN LC pump laser tuned to 800 nm and with a double-peaked (off resonance, see Fig. 1b) Yb-laser spectrum. Scalebar on each figure: 50 µm.

4. References

[1] D. Haluszka, K. Lőrincz, N. Kiss, R. Szipőcs, E. Kuroli, N. Gyöngyösi, N. Wikonkál, "Diet-induced obesity skin changes monitored by in vivo SHG and ex vivo CARS microscopy," Biomed. Opt. Express **7**, 4480–4489 (2016).
[2] A. Duarte, C. Schnedermann, P. Kukura, "Wide-Field Detected Fourier Transform CARS Microscopy,"Scientific Reports **6**, 37516 (2016).
[3] G. Molnár, Á. Krolopp, N. Kiss, G. Tamás, R. Szipőcs, "Interferometric Spectral Modulation of sub-100-fs Pump Pulses for High Chemical Contrast, Background Free, Real Time CARS Imaging," Biomedical Optics Congress 2018, OSA Technical Digest, paper JTh3A.29 (2018)
[4] N. Kiss, Á. Krolopp, K. Lőrincz, A. Bánvölgyi, R. Szipőcs, and N. Wikonkál, "Stain-free Histopathology of Basal Cell Carcinoma by Dual Vibration Resonance Frequency CARS Microscopy," Pathol. Oncol. Res. **24**, 927-930 (2018).
[5] A. Ozsvár, R. Szipőcs, Z. Ozsvár, J. Baka, P. Barzó, G. Tamás, and G. Molnár, "Quantitative analysis of lipid debris accumulation caused by cuprizone induced myelin degradation in different cns areas," Brain Research Bulletin **137**, 277-284 (2018).
[6] P. Antal, R. Szipőcs, "Tuneable, low-repetition-rate, cost-efficient femtosecond Ti:sapphire laser for nonlinear microscopy," Appl. Phys. B**107**, 17-22 (2012).

Biophotonics Congress: Optics in the Life Sciences 2021
(BODA,BRAIN,NTM,OMA,OMP) © OSA 2021

Fiber-coupled, 20 MHz Repetition Rate, sub-ps Ti:sapphire Laser for *in vivo* Nonlinear Microscopy of the Skin

Ádám Krolopp[1,2], Luca Fésűs[1,3], Gergely Szipőcs[2], Norbert Wikonkál[1,3] and Róbert Szipőcs[1,2,*]
[1] *Wigner RCP, Institute for Solid State Physics and Optics, P.O. Box 49, H-1525 Budapest, Hungary*
[2] *R&D Ultrafast Lasers Ltd, Konkoly-Thege str 29-33, H-1121 Budapest, Hungary*
[3] *Department of Dermatology, Venereology and Dermatooncology, Semmelweis University, Budapest, Hungary*

**Author e-mail address: r.szipocs@szipocs.com*

Abstract: A fiber coupled, sub ps Ti:sapphire laser suitable for *in vivo,* stain free, 3D imaging of skin alterations is introduced. It is pumped by a low cost, 2.1 W pump laser and delivers 0.6 1 ps high peak power pulses optimized for fiber delivery.

1. Introduction

Nonlinear microscopy, such as two-photon excitation fluorescence microscopy (2PEF), second-harmonic generation (SHG) microscopy and Coherent anti-stokes Raman scattering (CARS) microscopy is increasingly used to perform non-invasive, *in vivo* studies in life sciences. These techniques enable us to investigate the morphology or monitor the physiological processes (e.g. monitoring drug delivery) in the skin [1] by the use of ultrafast pulse lasers. Recent years brought revolutionary progress in the development of sub-ps pulse, all-fiber laser oscillators and amplifiers being suitable for nonlinear microscopy. Fiber (or fiber coupled) lasers are of great interest because they can easily be combined with endoscopy. This latter feature greatly increases the utility of nonlinear microscopy for pre-clinical applications and tissue imaging. In 2016, we reported on a novel, handheld 2PEF/SHG microscope imaging system comprising a sub-ps Yb-fiber laser system [2], which was suitable for *in vivo* imaging of murine skin at an average power level as low as 5 mW at 200 kHz sampling rate. The whole nonlinear microscope imaging system had the main advantages of the low price of the fs laser, fiber optics flexibility, a relatively small, light-weight scanning and detection head, and a very low risk of thermal or photochemical damage of the skin samples.

In principle, 2PEF microscopy can visualize endogenous fluorophores, such as elastin, keratin, NADH, FAD, etc., while the morphology of collagen fibers can be assessed by SHG microscopy. Due to the limited photon energy of our Yb-fiber laser system operating at around 1030 nm, however, we could not efficiently excite a few of these endogenous fluorophores (such as elastic fibers, NADH, FAD) with our handheld our 2PEF imaging system. This fact considerably limited its applicability in case of rear skin diseases (such as Ehlers-Danlos syndrome (EDS) [3], pseudoxanthoma elasticum (PXE) [4]) or in case of basal cell carcinoma (BCC) [5], the latter one being the most common malignancy in Caucasians. In order to overcome this problem, we replaced our Yb-fiber laser by a fiber coupled Ti:sapphire laser operating at around 810 nm, whose physical parameters (repetition rate, spectral bandwith, peak intensity, etc) were optimized for fiber delivery and low thermal load, *in vivo* imaging of the skin.

2. Results

The ~ 20 MHz repetition rate (long cavity), sub-ps Ti:S laser used in our fiber delivery and nonlinear microscope imaging experiment is similar to that we used for real time histology of the skin by simultaneous CARS imaging of lipids and proteins [6]. The basic configuration of this long cavity was described in details in Ref. 7. For our imaging experiments, however, we had to make a few modifications in order to reduce the spectral bandwidth of the laser. It results in higher chemical selectivity in DVRF-CARS imaging [6] and lower sensitivity of the optical pulses for dispersive effects during fiber delivery. To this end, we replaced the SF10 prism pair by a piezo controlled Gires-Tournois interferometer (GTI), which provided considerably higher intracavity dispersion than a prism pair. A birefringent filter (BRF) is used for tuning of the laser. Owing to the enlarged intracavity dispersion, spectral bandwidth of the Ti:sapphire laser has been reduced below 2 nm. Accordingly, the pulse duration of the laser increased above 600 fs. This four-fold reduction in the peak intensity was compensated by the lower repetition rate of our long cavity Ti:sapphire laser comprising a Herriott-cell [7]. The laser is pumped by a 2.1 W average power, 532 nm laser (*Opus*, product of Laser Quantum, UK). Final setup of the 20 MHz repetition rate, sub-ps Ti:S laser used for fiber delivery and imaging experiment is shown in Fig. 1. Pulse duration of the ~20 MHz laser was characterized by a PulseCheck autocorrelator (APE GmbH, DE). Depending on the intracavity dispersion set by the mirror spacing of an intracavity GTI, the pulse duration could be set in the 0.6-1 ps range (see Fig. 2.a, black dots). The $\Delta\lambda < 2$ nm spectral bandwidth of the laser allows distortion free fiber delivery of the optical pulses through a

~1.8 m long HC-800-2 type, commercial hollow core photonic bandgap fiber with honeycomb structure (product of NKT Photonics, Denmark) (see Fig. 2.a, red dots). The mode-locked average power of the laser is ~225 mW, after the fiber decoupling optics it is reduced to ~125 mW.

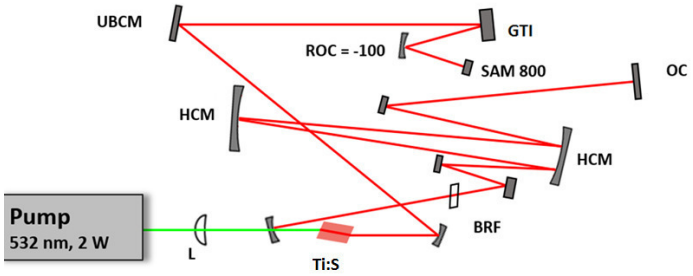

Fig. 1. Setup of the 20 MHz repetition rate sub-ps Ti:sapphire laser used for fiber delivery and nonlinear microscope imaging of the skin. Ti:S: Ti:sapphire crystal (PL= 4mm), BRF: birefringent filter for wavelength tuning, HCM: Herriott-cell mirros, UBCM: ultrabroadband chirped mirrors, GTI: a piezo-controlled Gires-Tournois interferometer, SAM 800: saturable absorber mirror, OC: output coupler.

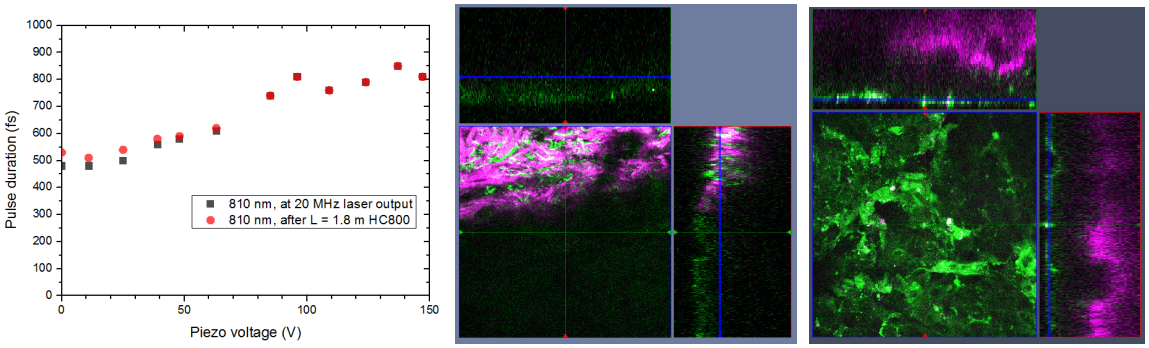

(a) (b) (c)

Fig. 2. (a) Pulse duration of the laser vs. piezo voltage of GTI measured before (black dots) and after (red dots) a 1.8 m hollow core fiber. (b) Tumor border of BCC and (c) hemangioma detected by SHG imaging of collagen and TPEF measuerement in the 500-550 nm spectral range. Laser central wavelength: 810 nm. Average power on sample: ~20 mW. Image size: 420 x 420 μm^2. Z-stack imaging range: 0-180 µm.

Fresh and frosen skin biopsies of different skin alterations (hemangioma, BCC and PXE) have been used for testing our fiber-coupled laser for z-stack imaging. In case of BCC [5], we could detect the border of the tumor highlighted by a strong contrast of AF (cells with basal cell morphology) and SHG (collagen fibers around tumor nest). In case of hemangioma, that is a benign proliferation of capillaries, we could observe superficial AF signal corresponding to capillaries. In case of PXE [4], however, we could not detect calcification, since our imaging depth of ~200 µm was not sufficient to reach the region of calcification, which is typically located in the mid-dermis at least 300 µm below the skin surface.

References

[1] A. Kolonics, Z. Csiszovszki, E. R. Tőke, O. Lőrincz, D. Haluszka, and R. Szipőcs, "*In vivo* study of targeted nanomedicine delivery into Langerhans cells by multiphoton laser scanning microscopy," Exp. Dermatol. **23**(8), 596–605 (2014).

[2] Á. Krolopp, A. Csákányi, D. Haluszka, D. Csáti, L. Vass, A. Kolonics, N. Wikonkál, and R. Szipőcs, "Handheld nonlinear microscope system comprising a 2 MHz repetition rate, mode-locked Yb-fiber laser for *in vivo* biomedical imaging," Biomed. Opt. Express **7**(9), 3531–3542 (2016).

[3] N. Kiss, D. Haluszka, K. Lőrincz, E. Kuroli, J. Hársing, B. Mayer, S. Kárpáti, G. Fekete, R. Szipőcs, N. Wikonkál and M. Medvecz, "*Ex vivo* nonlinear microscopy imaging of Ehlers-Danlos syndrome-affected skin," Arch. Dermatol. Res. **310**(5), 463-473 (2018).

[4] N. Kiss, L. Fésűs, S. Bozsányi, F. Szeri, M. Van Gils, V. Szabó, A.I. Nagy, B. Hidvégi, R. Szipőcs, et al. "Nonlinear optical microscopy novel tool for the analysis of cutaneous alterations in pseudoxanthoma elasticum," ," Lasers in Medical Science **35,** 1821-1830 (2020).

[5] N. Kiss, D. Haluszka, K. Lőrincz, S. Bozsányi, N. Wikonkál, and R. Szipőcs, "Quantitative Analyses on Second Harmonic Generation Microscopy Images of Collagen in *Ex Vivo* Basal Cell Carcinoma Samples in Comparison to Normal Skin," in Biophotonics Congress: Biomedical Optics 2018 (Optical Society of America, 2018), paper JW3A.12.

[6] L. Fésűs, Á. Krolopp, G. Molnár, N. Kiss, G. Tamás, and R. Szipőcs, "A 20 MHz, sub-ps, Tunable Ti:sapphire Laser System for Real Time, Stain Free, High Contrast Histology of the Skin," in Biophotonics Congress: Biomedical Optics 2020 (OSA, 2020) paper MTh3A.4.

[7] P. Antal, R. Szipőcs, "Tunable, low-repetition-rate, cost-efficient fs Ti:S laser for nonlinear microscopy," Appl. Phys. B**107**, 17-22 (2012).

European Conferences on Biomedical Optics 2021 (ECBO) © OSA-SPIE 2021

Numerical Analysis on *ex vivo* Second Harmonic Generation Images of Collagen Structure of Unstained Basal Cell Carcinoma Sections

Luca Fésűs[1,2], Norbert Wikonkál[1,2], Róbert Szipőcs[1,*]
[1] *Wigner RCP, Institute for Solid State Physics and Optics, P.O. Box 49, H-1525 Budapest, Hungary*
[2] *Department of Dermatology, Venereology and Dermatooncology, Semmelweis University, Budapest, Hungary*
**Author e-mail address: r.szipocs@szipocs.com*

Abstract: FFT analysis on mosaic SHG images of basal cell carcinoma skin sections of different subtypes is presented. This analysis combined with two-photon auto-fluorescence imaging might be useful for assessment of tumor borders.

1. Introduction

Basal cell carcinoma (BCC) is the most common malignancy in Caucasians [1]. Although BCCs rarely metastasize, local tissue degradation may lead to severe health and cosmetic damage and inoperability [2]. The gold standard in the therapy of BCC is surgical excision. However, BCCs often have poorly defined borders challenging complete excision [3]. Therefore, there is a demand for efficient imaging techniques for numerical evaluation of the tumor borders of BCC prior to and during surgery. Previously, second harmonic generation (SHG) nonlinear microscopy mosaic imaging was used to analyze collagen structure of BCC skin samples and increased collagen fiber length, decreased fiber angle and significantly higher fiber alignment of collagen fibers in BCC was found [4]. In this study, we carried out fast Fourier-transformation (FFT) analysis on mosaic SHG images from BCC skin sections of different subtypes (nodular, micronodular and invasive BCC). Our aim was to investigate if there are any differences in their collagen structure and to differentiate between subtypes according to the properties of collagen fibers, as well as to determine tumor borders. Our result shows that accuracy of FFT analysis highly depends on the unit cell size parameters (resolution, physical dimension of rectangular image portions) used for FFT. Furthermore, we found that collagen fibers around hair follicles give similar FFT results as fibers around tumor nests, which might hamper exact determination of tumor borders. Combination of FFT analysis with two-photon auto-fluorescence imaging, however, might offer a useful imaging tool for assessment of tumor borders of BCC.

2. Methods

4 pcs nodular, 4 pcs micro-nodular and 4 pcs infiltrative basal cell cancer samples were collected, formalin fixed and paraffin embedded, then 50 μm thick deparrafinized sections orthogonal to the skin surface were prepared from tissue blocks for SHG and TPEF imaging.

Nonlinear microscope images were captured by a commercial *Axio Examiner LSM 7 MP* laser scanning two-photon microscope (Carl Zeiss AG, Jena, Germany), with custom-modified detection optics for SHG imaging. For 2P excitation, a ~20 MHz repetition rate, tunable, sub-ps Ti:sapphire laser (*FemtoRose TUN LC GTI NoTouch*, R&D Ultrafast Lasers Ltd., Budapest, Hungary, see Ref. [5] for details) was used at an operation wavelength set to 800 nm. Violet (405/20 nm) and orange (590/40 nm) band-pass emission filters were respectively used to spectrally select TPEF and SHG signals. For focusing of the laser beam, a 20× water immersion objective (W-Plan – APOCHROMAT 20×/1,0 DIC (UV) VIS-IR, Carl Zeiss AG, Germany) was employed providing an imaging area of ~0.42 × 0.42 mm^2. Mosaic images were acquired by using a computer controlled, stepping motor driven X-Y positioning stage developed for tissue sections fixed on microscope slides (*Mosaic Positioning System*, R&D Ultrafast Lasers Ltd., Budapest, Hungary).

Fast Fourier Transformation (FFT) was carried out to measure the degree of organization and symmetry of collagen fibers [6]. FFT output images were converted to power plots for more accurate analysis [7]. As the eccentricity of the power plots reflects the arrangement of the collagen fibers, an ellipse was fitted to each power plot. In this study, we calculated collagen arrangement (CA) as the ratio of long axis/short axis of ellipse. A circular power plot reflects a normal skin sample where collagen shows an isotropic behavior, while an elongated power plot indicates parallelly oriented fibers [8]. FFT processing and image analysis were performed using a public domain image processing software (*ImageJ*). Individual (~0.42 × 0.42 mm^2) images were divided to 4 (2x2), 9 (3x3), 16 (4x4) or 25(5x5) even quadrangles (that we refer to as unit cells), for more precise spatial analysis. All unit cells with a total intensity

above a certain threshold went through FFT analysis. Threshold was chosen well above the background noise level. After calculation of long axis/short axis ratio (CA index), maximum value of CA index was truncated to 3 for better contrast in the corresponding "heat map", in which high (CA>2) ratios were assigned to „possibly tumorous" collagen and therefore were displayed in red color. Smaller (CA< 1,5) ratios were assigned to „healthy collagen" and were displayed in blue. Heat map plots were generated by using a *MATLAB* software.

3. Results

Collagen fiber pattern in 4 nodular, 4 micronodular and 4 infiltrative basal cell cancer sections were analyzed by our FFT method in order to determine CA ratio maps corresponding for each mosaic images. Our individual image resolution was set to 512x512 pixels during recording of mosaic images. A mosaic image comprises n by m individual images, where n and m take values in the 6 to 10 range depending the physical size of a skin section.

During the analysis of different division patterns, we found that division of individual images to 9 (3x3) unit cells gave the best results regarding resolution and accuracy in highlighting basal cell cancer tumor nests. If smaller images were FFT analyzed, differences in straight and curved fibers were less prominent. However, a small unit cell size is necessary to filter out small tumor nests (see Fig. 1).

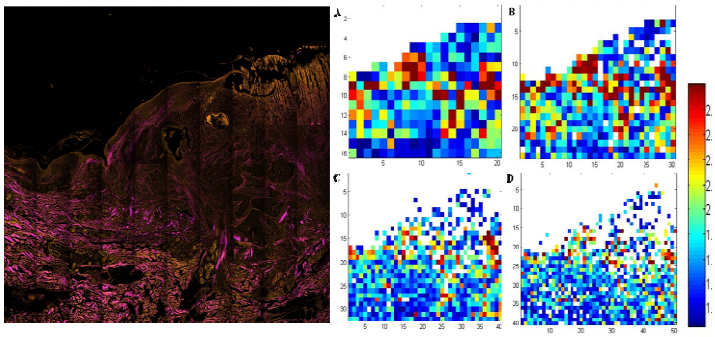

(a) (b)

Fig.1 (a) Stain-free two-photon mosaic image of a deparrafinized micronodular basal cell cancer section. Magenta: SHG signal of collagen, orange: TPEF autofluorescence singal. Mosaic image size: 4.2 mm (H) x 4.2 mm (V). Individual image size in mosaic image: 420x420 μm^2. (b) A-D: Heatmaps (CA ratio maps) calculated for different spatial resolution. An individual NLM image was divided to A: 2x2, B: 3x3, C: 4x4, D: 5x5 even quadrangles (unit cells) for FFT analysis to determine CA ratio maps.

We have also learned that thin collagen fibers are more difficult to analyze, which often results in false CA ratios (see Fig. 2). We found that small tumor nests have better visibility if they are surrounded by thicker collagen bundles. Big nodular basal cell carcinomas are less circumscribed if surrounding collagen fibers are thin even if they are quite parallelly oriented.

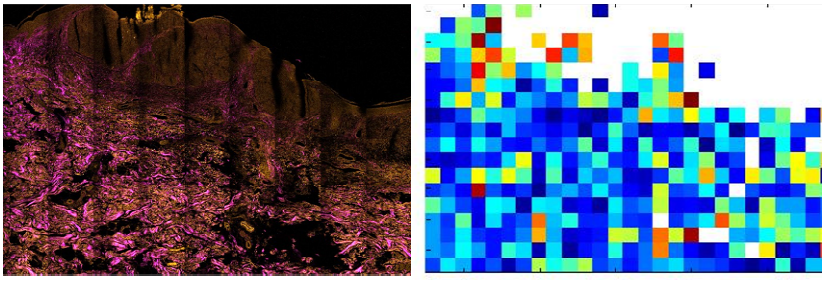

(a) (b)

Fig.2 (a) Mosaic image and (b) CA ratio heatmap generated for a nodular basal call cancer skin section with thin collagen fibers around tumor nests. Heatmap is calculated for 3x3 even quadrangles in an individual image resulting in a spatial resolution of 1.14 mm over the total mosaic image size of 4 mm x 3.2 mm. For color encoding and individual image size see Fig. 1.

Suprisingly, we have also found that collagen fibers around hair follicles result in similar CA ratios than fibers around tumor nests, which results from their oval/circular crossection. This hampers exact determination of tumor borders purely from SHG images of collagen (see Fig. 3).

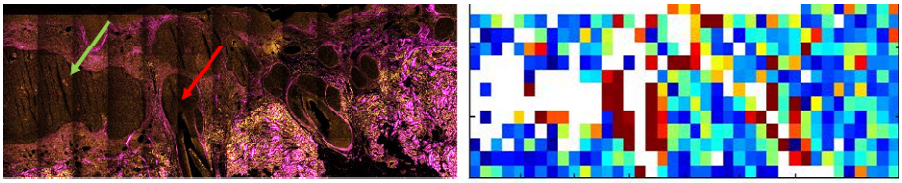

Fig.3. (a) Mosaic image and (b) CA ratio heatmap generated in case of hair follicle located at the edge of basal cell cancer. For color encoding and individual image size, see Fig. 1. Heatmap is calculated for 3x3 unit cells in an individual image.

4. Discussion

To date, a dermatoscope is routinely used imaging tool for the diagnosis of BCC providing a 10-fold magnification [9]. This cost-effective method increases diagnostic accuracy with 5-30% over visual inspection [10]. Tumor margins are difficult to be assessed by dermoscopy in case of superficial and infiltrative BCCs due to low magnification [3]. Nonlinear microscopy has been used for detection of BCC, where SHG and TPEF intensities were evaluated [11]. As the quantitative assessment approaches of the morphology of collagen fibers in BCC and healthy skin samples are not influenced by external factors, SHG imaging of collagen can be a promising method. Our numerical analysis of FFT transformed images revealed higher CA in the BCC samples around tumor nests compared to the healthy dermis, although we found some artifacts that have to be taken into account during evaluation of these numerical results.

Crossectional image of hair follicles and surrounding collagen fibers are prone to misinterpretation due to their similarly organized orientation to that around smaller tumor nests. SHG images itself do not provide information on cellular structure. However, if we record TPEF images of BCC sections additionally, distinghuising between basal cell cancer cells and hair follicle cells becomes feasible. Moreover, there are no hair follicles present inside a basal cell cancer, thus, presence of a hair follicle also indicates tumor border. Obviously, interpretation of SHG images without TPEF signal might be misleading. Accuracy of the FFT method presented highly depends on thickness of collagen fibers and size of the unit cells FFT analyzed. Especially in the case of nodular basal cell carcinoma, collagen fibers around the tumor nest are considerably thinner than healthy collagen bundles. This fact can be explaned by the structural transformation of collagen, which is characteristic for nodular basal cell carcinoma. Thus, in this case, FFT analysis might not result in adequate results. We provided our analysis for SHG images of skin sections normal to the skin surface. *In vivo* SHG imaging and FFT analysis of collagen structure might also face the problem of decreasing resolution of SHG images with increasing distance from the skin surface.

Quantitative image analysis including FFT combined with TPEF imaging can be integrated in handheld nonlinear microscope systems [12] comprising a fiber-coupled, cost efficient sub-ps laser source operating at around 800 nm [5] for diagnosis and assessment of tumor borders of BCC. According to issues listed above, however, further research is needed to verify its utility for diagnosis and therapy of BCC or other skin lesions.

5. References

[1] G. Goldenberg, T. Karagiannis, J.B. Palmer, J. Lotya, C. O'Neill, R. Kisa, V. Herrera, D.M. Siegel "Incidence and prevalence of basal cell carcinoma (BCC) and locally advanced BCC (LABCC) in a large commercially insured population in the United States: a retrospective cohort study," J Am Acad Dermatol **75**, 957–966 (2016).
[2] A. Crowson, "Basal cell carcinoma: biology, morphology and clinical implications," Mod Pathol **19**, S127–S147 (2006).
[3] S. Seidenari, F. Arginelli, S. Bassoli, et. al."Diagnosis of BCC by multiphoton laser tomography," Skin Res Technol 19(1) (2013).
[4] N. Kiss, D. Haluszka, K. Lőrincz, N. Gyöngyösi, S. Bozsányi, A. Bánvögyi, R. Szipőcs, N. Wikonkál, "Quantitative analysis on *ex vivo* nonlinear microscopy images of basal cell carcinoma samples in comparison to healthy skin," Pathol Oncol Res **25**, 1015–1021 (2019).
[5] A. Krolopp, L. Fésűs, G. Szipőcs, N. Wikonkál and R. Szipőcs "Fiber-coupled, 20 MHz repetition rate, sub-ps Ti:sapphire laser for *in vivo* nonlinear microscopy of the skin," submitted to ECBO 2021, Control ID: 3567062 (2021).
[6] W. James, P. Cooley, D. Peter "Historical notes on the fast Fourier transform," Proc IEEE 55(10):1675 (1967).
[7] K. Lu, J. Chen, S. Zhuo, L. Zheng, X. Jiang, X. Zhu, J. Zhao "Multiphoton laser scanning microscopy of localized scleroderma," Skin Res Technol **15**, 489–495 (2009).
[8] S. Wu, H. Li, H. Yang, X. Zhang, Z. Li, S. Xu "Quantitative analysis on collagen morphology in aging skin based on multiphoton microscopy," J Biomed Opt **16**, 040502 (2011).
[9] G. Argenziano, H. Soyer, S. Chimenti, et al. "Dermoscopy of pigmented skin lesions: results of a consensus meeting via the internet. J Am Acad Dermatol **48**, 679–693 (2003).
[10] R. Braun, H. Rabinovitz, M. Olivier, A. Kopf, J. Saurat "Dermoscopy of pigmented skin lesions," J Am Acad Dermatol **52**, 109–121 (2005).
[11] S. Lin, S. Jee, C. Kuo, R. Wu, W. Lin, J. Chen, Y. Liao, C. Hsu, T. Tsai, Y. Chen, C. Dong "Discrimination of basal cell carcinoma from normal dermal stroma by quantitative multiphoton imaging," Opt Lett **31**, 2756–2758 (2006).
[12] A. Krolopp, A. Csakanyi, D. Haluszka, D. Csati, L. Vass, A. Kolonics, N. Wikonkal, R. Szipocs "Handheld nonlinear microscope system comprising a 2 MHz repetition rate, mode-locked Yb-fiber laser for *in vivo* biomedical imaging," Biomed Opt Express **7**, 3531–3542 (2016).